Approximating Input-Output Curve of Pumped Storage Hydro Plant: A Disjunctive Convex Hull Method

Siyuan Wang, Jian Liu, Rui Bo, *Senior Member, IEEE*, Yonghong Chen, *Senior Member, IEEE*

***Abstract*—Pumped storage hydro (PSH) plant is a valuable resource with storage and fast ramp capabilities, which can manage the intermittency of renewable energy. An accurate model for the input-output curve of PSH plant can capture its varying efficiency feature and enable accurate evaluations of available generating/pumping capability. However, the trade-off between approximation accuracy and computation time poses a significant challenge for input-output curve modeling. In this paper, we develop a hypograph-relaxation-based input-output curve modeling framework, wherein sufficient conditions for exact hypograph relaxation are defined, proved, and analyzed for fixed-speed PSH considering the value of water in the upper reservoir. Under this framework, a novel disjunctive convex hull model is proposed to balance the aforementioned trade-off. Our model can take advantage of high accuracy in time-consuming piece-wise approximation models, and acceptable computation burden in less-accurate convex hull models. To divide a given input-output curve into various components that can be approximated by their respective convex hulls, we propose to use an approximate convex decomposition (ACD) based approach. The proposed model is tested for profit maximization problems using real-world Ludington PSH station data. Numerical results demonstrated the superior computational advantage of the proposed approach.**

***Index Terms*—Pumped storage hydro, input-output curve, hypograph relaxation, disjunctive convex hull, mixed-integer linear program.**

NOMENCLATURE

Indices and Sets

t, h, r	Index for time periods, PSH units, and reservoirs.
$\mathcal{T}, \mathcal{R}$	Set of time periods and reservoirs.
$\mathcal{H}_r$	Set of PSH units that are connected to upper reservoir r.
$\mathcal{I}_h^{\mathrm{g}}, \mathcal{I}_h^{\mathrm{p}}$	Set of convex components for generating and pumping modes of PSH unit h.
$\mathcal{K}_i, \mathcal{K}_i^{\mathrm{upper}}$	Set of inequalities, which represent planes, in convex component i and the upper convex hull of component i.
$\mathcal{L}_h^{\mathrm{g}}, \mathcal{L}_h^{\mathrm{p}}$	Set of binary variable indices ζ for generating and pumping modes of PSH unit h.

Parameters and Functions

N_t	Number of time periods.
Δt	Length of each time period.
$\underline{P}_h^{\mathrm{g}}, \overline{P}_h^{\mathrm{g}}$	Minimum and maximum generating power for PSH unit h.
$\underline{Q}_h^{\mathrm{g}}, \overline{Q}_h^{\mathrm{g}}$	Minimum and maximum flow rate for PSH unit h in the generating mode.
$\underline{P}_h^{\mathrm{p}}, \overline{P}_h^{\mathrm{p}}$	Minimum and maximum pumping power for PSH unit h.
$\underline{Q}_h^{\mathrm{p}}, \overline{Q}_h^{\mathrm{p}}$	Minimum and maximum flow rate for PSH unit h in the pumping mode.
$\underline{V}_r, \overline{V}_r$	Minimum and maximum water volume for reservoir r.
$\hat{q}_{r,t}^{\mathrm{infl}}, \hat{q}_{r,t}^{\mathrm{outfl}}$	Flow rate for natural inflow to and outflow from reservoir r in time period t.
$\hat{\lambda}_{h,t}$	Locational marginal price forecast for PSH unit h in time period t.
$\varphi_h^{\mathrm{g}}(\cdot), \varphi_h^{\mathrm{p}}(\cdot)$	Input-output curve function for generating and pumping modes of PSH unit h.
$vow_r(\cdot)$	Value-of-water function for reservoir r.
$\gamma_{h,i,k}^{\mathrm{pg}}, \gamma_{h,i,k}^{\mathrm{qg}}, \gamma_{h,i,k}^{\mathrm{vg}}, \gamma_{h,i,k}^{0}$	Coefficients for the k-th inequality in convex component i of PSH unit h for the generating mode.
$\tau_{h,i,k}^{\mathrm{qp}}, \tau_{h,i,k}^{\mathrm{vp}}, \tau_{h,i,k}^{0}$	Coefficients for the k-th inequality in convex component i of PSH unit h for the pumping mode.

Decision Variables

$u_{h,t}^{\mathrm{g}}, u_{h,t}^{\mathrm{p}}$	Binary generating and pumping status variables for PSH unit h in time period t.
$p_{h,t}^{\mathrm{g}}, p_{h,t}^{\mathrm{p}}$	Generating and pumping power for PSH unit h in time period t.
$q_{h,t}^{\mathrm{g}}, q_{h,t}^{\mathrm{p}}$	Generating and pumping flow rate for PSH unit h in time period t.
$v_{r,t}$	Volume of water in reservoir r at the end of time period t.
$s_{r,t}$	Spillage from reservoir r in time period t.
$\phi_{h,t,i}^{\mathrm{g}}, \phi_{h,t,i}^{\mathrm{p}}$	Selection variable for convex component i of PSH unit h at time period t for the generating and pumping modes (i.e, if component i is selected, $\phi_{h,t,i}^{(\cdot)} = 1$; otherwise, $\phi_{h,t,i}^{(\cdot)} = 0$).
$\zeta_{h,t,\ell}^{\mathrm{g}}, \zeta_{h,t,\ell}^{\mathrm{p}}$	Binary variables to ensure $\phi_{h,t,i}^{\mathrm{g}}$ (or $\phi_{h,t,i}^{\mathrm{p}}$) values are mutually exclusive of each other.
$p_{h,t,i}^{\mathrm{g}}(q_{h,t,i}^{\mathrm{g}}, v_{h,t,i}^{\mathrm{g}})$	Power (flow rate, volume) ancillary variables that correspond to convex component i in the generating mode for PSH unit h.

This material is based upon work supported by the U.S. Department of Energy's Office of Energy Efficiency and Renewable Energy (EERE) under the Water Power Technologies Office Award Number DE-EE0008781. Paper no. TPWRS-00685-2021. *(Corresponding Author: Rui Bo.)*

S. Wang, J. Liu, and R. Bo are with the Department of Electrical and Computer Engineering, Missouri University of Science and Technology, MO 65409 USA (e-mail: siyuanwang@mst.edu; jliu@mst.edu; rbo@mst.edu).

Y. Chen is with Midcontinent Independent System Operator, Inc., Carmel, IN 46032 USA (e-mail: ychen@misoenergy.org).

This article has been accepted for publication in IEEE Transactions on Power Systems. DOI: 10.1109/TPWRS.2022.3158629.

$q^{\mathrm{p}}_{h,t,i}(v^{\mathrm{p}}_{h,t,i})$ Flow rate (volume) ancillary variables that correspond to convex component i in the pumping mode for PSH unit h.

$v^{\mathrm{i}}_{h,t}$ Volume ancillary variable that corresponds to the idle mode for PSH unit h.

I. Introduction

WITH increasing penetration of renewable energy in power systems worldwide, pumped storage hydro (PSH), as the most widely used utility-scale storage, plays an important role to address renewable energy uncertainties. Accurate modeling of PSH plants is instrumental in ensuring the best utilization of PSH storage capability and dispatch flexibility. Conventionally, head-independent constant energy conversion efficiency factors have been widely adopted to model PSH plants in the literature [1]–[5]. However, real-world data reveals PSH plant efficiency varies considerably with water head and operating point, therefore constant efficiency assumption may lead to considerable errors and inefficiency in PSH operation and handling of renewable energy uncertainty [6]. It warrants more accurate modeling of the energy conversion efficiency. However, significant modeling and computational challenges are encountered.

The input-output curve is used to describe the relations of generating/pumping power, flow rate, and reservoir volume (or net head). Although nonlinear programming (NLP) approaches are used to deal with this nonlinear and non-convex curve in related works such as [6], mixed-integer linear programming (MILP) serves as a state-of-art tool in the industry, as well-designed MILP models can be efficiently solved by on-the-shelf commercial solvers in a timely and reliable manner. In previous works, there are two mainstream approaches to model input-output curves (or production curves) for PSH and conventional hydro with MILP. For convenience, we use a two-dimensional curve $y = \varphi_h(x)$ shown in Fig. 1 to conceptually illustrate the related methods.

1) The first category is piece-wise linear approximation methods. We start with conventional hydro units, for which this kind of approach was developed earlier. Authors of [7]–[9] use a two-step piece-wise linear approximation method, which addresses the input-output under each head level first, and then determines the power from a given head level. A direct three-dimensional piece-wise linear approximation method is proposed in [10], and used for a hydro-thermal unit commitment problem in [11]. The authors of [12] comprehensively summarize the piece-wise linear approximation approaches for conventional hydro production function modeling, and conclude the logarithmic modeling method in [13] has the best performance at that time. For PSH units, the value of detailed input-output curve modeling is analyzed in [14]. An early work in [15] assumes the input-output curve is convex. The piece-wise linear approximation method in [7]–[9] are then applied to PSH input-output curve modeling in [14], [16], [17]. We recently proposed to use a zig-zag piece-wise approximation approach [18], [19] to model the PSH input-output curve in [20], which can further reduce the solution time for time-intensive cases in comparison to the logarithmic method in [12]. This method can potentially be applied to conventional hydro modeling. As indicated in Fig. 1a, the accuracy of the piece-wise linear approximation can be enhanced with an increased number of pieces, meanwhile the computational burdens also increase due to the inclusion of more integer variables.

2) An alternative kind of approach is convex hull approximation, which has only been applied to conventional hydro modeling now. The convex hull approximation approach is proposed for input-output curve modeling in dispatching a centralized Brazilian hydro system in [21]. This input-output curve model is purely linear without the inclusion of integer variables. However, as illustrated in Fig. 1b, this method may suffer from accuracy issues in approximating non-concave portion of the curve. Furthermore, the approximation accuracy of the convex hull approximation cannot be improved by increasing the number of linear constraints. Note this approach in fact relax the feasible region of an input-output curve to its convex hull. For both conventional hydro and PSH input-output curve modeling, how to apply similar relaxation approaches to reduce the use of integer variables, meanwhile ensuring acceptable accuracy, is needed to investigate. Moreover, whether the optimal solution still falls on the original curve is unknown when we apply similar relaxation approaches to PSH modeling.

In this work, we first propose a hypograph relaxation method to model input-output curves of fixed-speed PSH units. The term "hypograph relaxation" means relaxing the input-output curve to its hypograph. Taking $y = \varphi_h(x)$ in Fig. 1c as

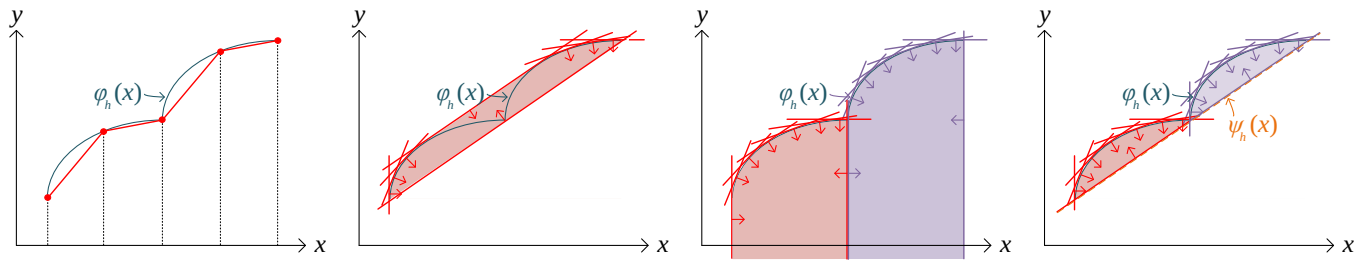

Fig. 1. A comparison of modeling methods: (a) piece-wise linear modeling, (b) convex hull modeling, (c) disjunctive convex hull modeling (to explain the concept "hypograph relaxation"), (d) disjunctive convex hull modeling (in our implementation). Note the figures here are only used for conceptual illustration purposes. They do not necessarily present what the realistic input-output curves look like.

an illustrative example, the union of red and purple shadowed regions described by $y \leq \varphi_h(x)$, is the hypograph of $\varphi_h(x)$. In practice, y is usually downward bounded (such as constraints for minimum technical power, and constraints generated by convex hull). As shown in Fig. 1d, the union of red and purple shadowed regions described by $\psi_h(x) \leq y \leq \varphi_h(x)$, is technically a subset of the hypograph of $\varphi_h(x)$. For convenience, in this article, we also refer this as hypograph relaxation.

Furthermore, we also find the proposed hypograph relaxation formulation is exact under some sufficient conditions. Then, a novel disjunctive convex hull model to describe the hypograph relaxed feasible region, as conceptually illustrated in Fig. 1d, is proposed for input-output curves. In comparison to direct piece-wise linear approximation methods, the proposed method exploits the partially concave properties of the input-output curve to reduce the number of integer variables. Meanwhile, we take advantage of the integer variable modeling to preserve approximating accuracy for the non-concave portion of the curve, which can better address the accuracy issue over the convex hull approximation method. In our numerical simulation, we compare our proposed disjunctive convex hull model with the zig-zag integer piece-wise linear approximation method [20] and the purely convex hull approximation method [21].

When using our proposed disjunctive convex hull modeling approach, we need to calculate a high-quality partition to divide an input-output curve (or its hypograph relaxation) into several concave components (or convex subsets for the hypograph relaxation). This is similar to convex decomposition in the field of computer graphics. Exact convex decomposition was proposed by early works in [22], [23], which however suffers from generating an unmanageable amount of convex components [24], thus might tremendously increase the number of binary variables in our proposed disjunctive convex hull modeling approach. The idea of approximate convex decomposition (ACD) is to offer partitions with a small number of components, while the approximation accuracy can be controlled by predefined concavity metrics. A two-dimensional ACD algorithm for polygons is first proposed in [24], after which three-dimensional ACD approaches for polyhedron or polygon mesh are further proposed in [25], [26]. As the metric design in the algorithm varies from applications, in this work, we use a power-approximation-error based metric for our ACD process. The resultant partition can balance the approximation accuracy and the number of components for input-output curve modeling.

The main contributions of this work are in the following,

- We propose a hypograph relaxation for fixed-speed PSH input-output curve modeling, by extending the approach in [21]. Sufficient conditions for exact hypograph relaxation in our optimization problem are provided, and the applicability of these conditions is discussed.
- A disjunctive convex hull model is proposed for PSH input-output curve approximation, which leverages the advantages of the aforementioned two categories of approaches in the literature review. It can reduce the solution time under the same level of approximating accuracy.
- Customized ACD approaches are used to offer reasonable feasible-region partitions for our proposed input-output curve modeling approach.

II. Hypograph Relaxation of Input-output Curve

In this section, we first present a hypograph relaxed PSH model, which can be used in PSH owners' profit maximization. Sufficient conditions for exact hypograph relaxation in our optimization problem are defined, proved, and further discussed.

A. PSH Model and Hypograph Relaxation

As units in a PSH plant are usually connected to a single upper reservoir, here we show a model for an upper reservoir indexed with r. To apply this to systems with multiple PSH plants, the range of r can be extended to $\forall r \in \mathcal{R}$.

1) Power Constraints: The net power output, generating power bound, and pumping power bound constraints are presented in (1a), (1b) and (1c), respectively. Flow rate constraints for the generating and pumping modes are defined in (1d) and (1e), respectively. Equation (1f) is used to avoid simultaneously generating and pumping. Binary variables are declared in (1g).

$$p_{h,t} = p^{\mathrm{g}}_{h,t} - p^{\mathrm{p}}_{h,t} \qquad \forall h \in \mathcal{H}_r,\ \forall t \in \mathcal{T} \tag{1a}$$

$$\underline{P}^{\mathrm{g}}_h \cdot u^{\mathrm{g}}_{h,t} \leq p^{\mathrm{g}}_{h,t} \leq \overline{P}^{\mathrm{g}}_h \cdot u^{\mathrm{g}}_{h,t} \qquad \forall h \in \mathcal{H}_r,\ \forall t \in \mathcal{T} \tag{1b}$$

$$\underline{P}^{\mathrm{p}}_h \cdot u^{\mathrm{p}}_{h,t} \leq p^{\mathrm{p}}_{h,t} \leq \overline{P}^{\mathrm{p}}_h \cdot u^{\mathrm{p}}_{h,t} \qquad \forall h \in \mathcal{H}_r,\ \forall t \in \mathcal{T} \tag{1c}$$

$$\underline{Q}^{\mathrm{g}}_h \cdot u^{\mathrm{g}}_{h,t} \leq q^{\mathrm{g}}_{h,t} \leq \overline{Q}^{\mathrm{g}}_h \cdot u^{\mathrm{g}}_{h,t} \qquad \forall h \in \mathcal{H}_r,\ \forall t \in \mathcal{T} \tag{1d}$$

$$\underline{Q}^{\mathrm{p}}_h \cdot u^{\mathrm{p}}_{h,t} \leq q^{\mathrm{p}}_{h,t} \leq \overline{Q}^{\mathrm{p}}_h \cdot u^{\mathrm{p}}_{h,t} \qquad \forall h \in \mathcal{H}_r,\ \forall t \in \mathcal{T} \tag{1e}$$

$$u^{\mathrm{g}}_{h,t} + u^{\mathrm{p}}_{h',t} \leq 1 \qquad \forall h, h' \in \mathcal{H}_r,\ \forall t \in \mathcal{T} \tag{1f}$$

$$u^{\mathrm{g}}_{h,t}, u^{\mathrm{p}}_{h,t} \in \{0,1\} \qquad \forall h \in \mathcal{H}_r,\ \forall t \in \mathcal{T} \tag{1g}$$

If units that share the same upper reservoir are identical, we include constraints in (2a) and (2b) to break the symmetry. The rules for both generating and pumping modes are: lower-priority units should not start up if higher-priority units could be online, and higher-priority units should not shut down if lower-priority units could be offline.

$$u^{\mathrm{g}}_{h',t} - u^{\mathrm{g}}_{h',t-1} \leq u^{\mathrm{g}}_{h,t},\ u^{\mathrm{p}}_{h',t} - u^{\mathrm{p}}_{h',t-1} \leq u^{\mathrm{p}}_{h,t} \qquad \forall h, h' \in \mathcal{H}_r, h' = h+1,\ \forall t \in \mathcal{T} \tag{2a}$$

$$u^{\mathrm{g}}_{h,t-1} - u^{\mathrm{g}}_{h,t} \leq 1 - u^{\mathrm{g}}_{h',t},\ u^{\mathrm{p}}_{h,t-1} - u^{\mathrm{p}}_{h,t} \leq 1 - u^{\mathrm{p}}_{h',t} \qquad \forall h, h' \in \mathcal{H}_r, h' = h+1,\ \forall t \in \mathcal{T} \tag{2b}$$

2) Energy Constraints: For the the upper reservoir, detailed water balance constraint between consecutive time periods is defined in (3a). The upper and lower bounds for water volume are constrained in (3b). A trivial non-negative constraint for water spillage is shown in (3c).

$$v_{r,t} = v_{r,t-1} - \sum\nolimits_{h \in \mathcal{H}_r} q^{\mathrm{g}}_{h,t} \cdot \Delta t + \sum\nolimits_{h \in \mathcal{H}_r} q^{\mathrm{p}}_{h,t} \cdot \Delta t + \hat{q}^{\mathrm{infl}}_{r,t} \cdot \Delta t - \hat{q}^{\mathrm{outfl}}_{r,t} \cdot \Delta t - s_{r,t} \qquad \forall t \in \mathcal{T} \tag{3a}$$

$$\underline{V}_r \leq v_{r,t} \leq \overline{V}_r \qquad \forall t \in \mathcal{T} \tag{3b}$$

$$s_{r,t} \geq 0 \qquad \forall t \in \mathcal{T} \tag{3c}$$

3) Input-Output Curve Constraints: The input-output curve describes the relations of generating/pumping power, flow rate, and reservoir volume. Abstract equations for generating and pumping modes are represented in (4a) and (4b), respectively. The pumping power is assumed to be a fixed value when a fixed-speed PSH unit is operating in the pumping mode. Thus, the flow rate is modeled as a function of upper reservoir volume in (4b). In the literature, both volume at the beginning and end of time period t (i.e., $v_{r,t-1}$ and $v_{r,t}$, respectively) have been used to estimate the volume in time period t. We use $v_{r,t-1}$ in this work.

$$p^{\mathrm{g}}_{h,t} = \varphi^{\mathrm{g}}_h(q^{\mathrm{g}}_{h,t}, v_{r,t-1}) \quad \forall h \in \mathcal{H}_r,\ \forall t \in \mathcal{T} \tag{4a}$$

$$q^{\mathrm{p}}_{h,t} = \varphi^{\mathrm{p}}_h(v_{r,t-1}) \quad \forall h \in \mathcal{H}_r,\ \forall t \in \mathcal{T} \tag{4b}$$

Convex hull approximations for the conventional hydro input-output curves were proposed in [21]. Note that approach in fact results in a convex relaxation of the original input-output curve (i.e., the curve is expanded to a larger feasible region as shown in Fig. 1b). In this work, we propose a hypograph relaxation, which is conceptually shown in Fig. 1d. Without loss of generality, the relaxed form is expressed in (5a) and (5b) with the assumptions $\psi^{\mathrm{g}}_h(q^{\mathrm{g}}_{h,t}, v_{r,t-1}) \le \varphi^{\mathrm{g}}_h(q^{\mathrm{g}}_{h,t}, v_{r,t-1})$, $\psi^{\mathrm{p}}_h(v_{r,t-1}) \le \varphi^{\mathrm{p}}_h(v_{r,t-1})$, $\forall h \in \mathcal{H}_r,\ \forall t \in \mathcal{T}$. Note the relaxed feasible region does not necessarily have to be convex. Fig. 1d illustrates an example in which the relaxed feasible region (union of red and purple shadowed areas) is not convex.

$$\psi^{\mathrm{g}}_h(q^{\mathrm{g}}_{h,t}, v_{r,t-1}) \le p^{\mathrm{g}}_{h,t} \le \varphi^{\mathrm{g}}_h(q^{\mathrm{g}}_{h,t}, v_{r,t-1}) \quad \forall h \in \mathcal{H}_r,\ \forall t \in \mathcal{T} \tag{5a}$$

$$\psi^{\mathrm{p}}_h(v_{r,t-1}) \le q^{\mathrm{p}}_{h,t} \le \varphi^{\mathrm{p}}_h(v_{r,t-1}) \quad \forall h \in \mathcal{H}_r,\ \forall t \in \mathcal{T} \tag{5b}$$

4) The Whole Problem Formulation: From PSH owners' perspective, a profit maximization formulation is presented in (6) given predicted locational marginal price (LMP) $\hat{\lambda}_{h,t}$. A value-of-water term is defined in the objective function (8) to assess the future profit under different levels of end volume v_{r,N_t}, which can be obtained through methods in [27], [28]. The value-of-water function $vow_r(\cdot)$ is monotonically non-decreasing, as more ending volume would result in no less future profit. With the input-output curve in (4) relaxed to its hypograph (or subset of its hypograph) in (5), the relaxed formulation is shown in (7).

$$\max \quad \mathrm{obj}_{\mathrm{PSH}} \tag{6a}$$

$$\text{s.t.} \quad (1), (2), (3), (4) \tag{6b}$$

$$\max \quad \mathrm{obj}_{\mathrm{PSHr}} \tag{7a}$$

$$\text{s.t.} \quad (1), (2), (3), (5) \tag{7b}$$

where,

$$\mathrm{obj}_{\mathrm{PSH\ (PSHr)}} = \sum\nolimits_{t\in\mathcal{T}} \sum\nolimits_{h\in\mathcal{H}_r} \Big(\hat{\lambda}_{h,t} \cdot p_{h,t} - c^{\mathrm{g}}_h(p^{\mathrm{g}}_{h,t}, u^{\mathrm{g}}_{h,t}) - c^{\mathrm{p}}_h(p^{\mathrm{p}}_{h,t}, u^{\mathrm{p}}_{h,t}) \Big) + vow_r(v_{r,N_t}) \tag{8}$$

For this profit maximization model, it's not clear whether the optimal solution from the relaxed formulation falls on the original input-output curve. We provide sufficient conditions for exact hypograph relaxation in subsection II-B.

B. Sufficient Conditions for Exact Hypograph Relaxation

The hypograph relaxation in (7) has the following property.

Property: *If conditions 1 and 2 are satisfied, the optimization problem* (7)*, in which input-output curves are relaxed through hypograph relaxation, has the same objective values with the corresponding unrelaxed problems in* (6)*.*

Condition 1: *function $p^{\mathrm{g}}_h = \varphi^{\mathrm{g}}_h(q^{\mathrm{g}}_h, v_r)$ is monotonically non-decreasing on both q^{g}_h and v_r.*

Condition 2: *function $q^{\mathrm{p}}_h = \varphi^{\mathrm{p}}_h(v_r)$ is monotonically non-increasing on v_r; and $\sum_{h\in\mathcal{H}_r} \left[\varphi^{\mathrm{p}}_h(v^{(1)}_r) - \varphi^{\mathrm{p}}_h(v^{(2)}_r)\right] \cdot \Delta t \le v^{(2)}_r - v^{(1)}_r$ is satisfied for any $v^{(1)}_r$, $v^{(2)}_r$ in their respective bounds and $v^{(1)}_r < v^{(2)}_r$.*

We provide an outlined proof here, which contains the solution recovery steps. More details in the appendix complete the proof.

Proof. We prove the property through contradiction. Suppose the proposed property is not true, the optimal objective value from the hypograph relaxed problem in (7) is strictly larger than that from the unrelaxed problem in (6), i.e., $\mathrm{obj}^*_{\mathrm{PSH}} < \mathrm{obj}^*_{\mathrm{PSHr}}$. Thus, there exists a set of optimal PSH schedule from the relaxed formulation that does not fall on the input-output curve, which means at least one of RHS inequalities strictly hold in (5)[1]. Let the optimal solution from the relaxed formulation (7) be $u^{\mathrm{g}*}_{h,t}$, $p^{\mathrm{g}*}_{h,t}$, $q^{\mathrm{g}*}_{h,t}$, $u^{\mathrm{p}*}_{h,t}$, $p^{\mathrm{p}*}_{h,t}$, $q^{\mathrm{p}*}_{h,t}$, $v^*_{r,t}$. Based on the solution of the relaxed formulation, we perform the following steps to generate another solution.

Step 1, set initial value $t = 1$. Define $v^*_{r,0} = v^{**}_{r,0} = v_{r,0}$.

Step 2, let $u^{\mathrm{g}**}_{h,t} = u^{\mathrm{g}*}_{h,t}$, $p^{\mathrm{g}**}_{h,t} = p^{\mathrm{g}*}_{h,t}$. When $u^{\mathrm{g}*}_{h,t} = 1$, check whether $(q^{\mathrm{g}*}_{h,t},\ v^{**}_{r,t-1},\ p^{\mathrm{g}*}_{h,t})$ satisfies $p^{\mathrm{g}*}_{h,t} = \varphi^{\mathrm{g}}_h(q^{\mathrm{g}*}_{h,t}, v^{**}_{r,t-1})$. If yes, let $q^{\mathrm{g}**}_{h,t} = q^{\mathrm{g}*}_{h,t}$; otherwise, get the smallest $q^{\mathrm{g}**}_{h,t}$ from solving $p^{\mathrm{g}**}_{h,t} = \varphi^{\mathrm{g}}_h(q^{\mathrm{g}}_{h,t}, v^{**}_{r,t-1})$. When $u^{\mathrm{g}*}_{h,t} = 0$, let $p^{\mathrm{g}**}_{h,t} = 0$.

Step 3, let $u^{\mathrm{p}**}_{h,t} = u^{\mathrm{p}*}_{h,t}$, $p^{\mathrm{p}**}_{h,t} = p^{\mathrm{p}*}_{h,t}$. When $u^{\mathrm{p}*}_{h,t} = 1$, check whether $(v^{**}_{r,t-1},\ q^{\mathrm{p}*}_{h,t})$ satisfies $q^{\mathrm{p}*}_{h,t} = \varphi^{\mathrm{p}}_h(v^{**}_{r,t-1})$. If yes, let $q^{\mathrm{p}**}_{h,t} = q^{\mathrm{p}*}_{h,t}$; otherwise, let $q^{\mathrm{p}**}_{h,t} = \varphi^{\mathrm{p}}_h(v^{**}_{r,t-1})$. When $u^{\mathrm{p}*}_{h,t} = 0$, let $q^{\mathrm{p}**}_{h,t} = 0$.

Step 4, calculate $v^{**}_{r,t}$ as shown in (9) by using updated $q^{\mathrm{g}**}_{h,t}$ and $q^{\mathrm{p}**}_{h,t}$.

$$v^{**}_{r,t} = v^{**}_{r,t-1} - \sum\nolimits_{h\in\mathcal{H}_r} q^{\mathrm{g}**}_{h,t} \cdot \Delta t + \sum\nolimits_{h\in\mathcal{H}_r} q^{\mathrm{p}**}_{h,t} \cdot \Delta t + \hat{q}^{\mathrm{infl}}_{r,t} \cdot \Delta t - \hat{q}^{\mathrm{outfl}}_{r,t} \cdot \Delta t - s^{**}_{r,t} \tag{9}$$

where,

$$s^{**}_{r,t} = \max \left\{ v^{**}_{r,t-1} - \sum\nolimits_{h\in\mathcal{H}_r} q^{\mathrm{g}**}_{h,t} \cdot \Delta t + \sum\nolimits_{h\in\mathcal{H}_r} q^{\mathrm{p}**}_{h,t} \cdot \Delta t + \hat{q}^{\mathrm{infl}}_{r,t} \cdot \Delta t - \hat{q}^{\mathrm{outfl}}_{r,t} \cdot \Delta t - \overline{V}_r,\ 0 \right\} \tag{10}$$

Step 5, if $t < N_t$, $t \leftarrow t + 1$, go to Step 2; otherwise, terminate.

In terms of the constraints, it can be easily verified that the generated solution $u^{\mathrm{g}**}_{h,t}$, $p^{\mathrm{g}**}_{h,t}$, $q^{\mathrm{g}**}_{h,t}$, $u^{\mathrm{p}**}_{h,t}$, $p^{\mathrm{p}**}_{h,t}$, $q^{\mathrm{p}**}_{h,t}$, $v^{**}_{r,t}$ satisfy the constraints for PSH in (1), (2), and (3). Importantly, the PSH schedule generation process in Steps 2 and 3 guarantees

[1]Because if all the RHS inequalities in (5) hold with equalities, the solution from the relaxed formulation is also a feasible solution for the unrelaxed formulation. This contradicts that the objective values from the two formulations are different.

that all the RHS inequalities in (5) hold with equalities, i.e., $p^{\mathrm{g}**}_{h,t} = \varphi^{\mathrm{g}}_h(q^{\mathrm{g}**}_{h,t}, v^{**}_{r,t-1})$ and $q^{\mathrm{p}**}_{h,t} = \varphi^{\mathrm{p}}_h(v^{**}_{r,t-1})$. This means the generated PSH schedule falls on the input-output curve. All the constraints in the profit maximization problem (6) are satisfied.

In terms of the objective value, the $p^{\mathrm{g}}_{h,t}$, $p^{\mathrm{p}}_{h,t}$, $u^{\mathrm{g}}_{h,t}$ and $u^{\mathrm{p}}_{h,t}$ related cost terms for PSH in both (6a) and (7a) (see (8) for detail) keep the same. Thus, only the value-of-water term might change. We assert (11) is satisfied, for which the detailed proof is provided in the appendix.

$$v^{**}_{r,t} \geq v^{*}_{r,t} \quad \forall t \in \mathcal{T} \tag{11}$$

Considering the value-of-water function $vow_r(\cdot)$ is monotonically non-decreasing, the value-of-water term in (8), which is related to the ending volume, does not decrease for the generated solution, i.e., $vow_r(v^{**}_{r,N_t}) \geq vow_r(v^{*}_{r,N_t})$. Thus, the generated solution results in an equal or better objective value, i.e., $\mathrm{obj}^{**}_{\mathrm{PSHr}} \geq \mathrm{obj}^{*}_{\mathrm{PSHr}}$. Given the generated solution is also a feasible solution for the unrelaxed formulation in (6), we have $\mathrm{obj}^{*}_{\mathrm{PSH}} \geq \mathrm{obj}^{**}_{\mathrm{PSHr}}$. Consequently, the optimal objective value from the unrelaxed formulation in (6) is larger greater than or equal to that from the relaxed formulation in (7), i.e., $\mathrm{obj}^{*}_{\mathrm{PSH}} \geq \mathrm{obj}^{*}_{\mathrm{PSHr}}$. This contradicts $\mathrm{obj}^{*}_{\mathrm{PSH}} < \mathrm{obj}^{*}_{\mathrm{PSHr}}$, which was obtained from our assumption previously. ∎

We have proved the proposed property. Under the given conditions, as the optimal objective values from the relaxed and unrelaxed formulations keep the same, the optimal solutions from unrelaxed formulations (6) are also optimal solutions for relaxed formulations (7). Note the reverse of this assertion may not hold, as the PSH schedule from the relaxed formulation (7) does not necessarily fall on the input-output curves in (4) if the possibility of multiple solutions is considered. However, an exact PSH solution that satisfies (4) can be recovered through Steps 1-5 in the proof.

Remark 1: The property still holds if symmetry breaking constraints in (2) are not incorporated.

Remark 2: For ISO's market clearing problem, if constraints for PSH units are modeled as in (1), (2), (3), (5), and the PSH related term in the objective function is $\sum_{t\in\mathcal{T}}\sum_{h\in\mathcal{H}_r}\left[c^{\mathrm{g}}_h(p^{\mathrm{g}}_{h,t}, u^{\mathrm{g}}_{h,t}) + c^{\mathrm{p}}_h(p^{\mathrm{p}}_{h,t}, u^{\mathrm{p}}_{h,t})\right] - vow_r(v_{r,N_t})$ for each $r \in \mathcal{R}$, the proposed property still holds, which can be proved in a similar way through contradiction.

C. Discussion on the Conditions

According to the law of conservation of energy, a larger volume of water in the upper reservoir has no smaller gravitational potential energy, which leads to no less generated power given a fixed flow rate. Likewise, power output doesn't decrease as flow rate increases given fixed volume. Thus, *Condition 1* is reasonable for input-output curves in the generating mode.

For the pumping mode, given fixed pumping power, pumping flow rate does not increase as the water head increases, which is also according to the law of conservation of energy. So, the monotonicity condition in *Condition 2* is satisfied for general input-output curves in the pumping mode. We check the condition $\sum_{h\in\mathcal{H}_r}\left[\varphi^{\mathrm{p}}_h(v^{(1)}_r) - \varphi^{\mathrm{p}}_h(v^{(2)}_r)\right]\cdot\Delta t \leq v^{(2)}_r - v^{(1)}_r$ with data from Ludington PSH station. As a fixed speed PSH station with six identical units, the condition is equivalent to (12) by defining n as the number of online units.

$$\begin{aligned}(v^{(2)}_r - v^{(1)}_r)\big/\big(\varphi^{\mathrm{p}}(v^{(1)}_r) - \varphi^{\mathrm{p}}(v^{(2)}_r)\big) \geq n\cdot\Delta t \\ \forall v^{(1)}_r, v^{(2)}_r \in [\underline{V}_r, \overline{V}_r], v^{(1)}_r < v^{(2)}_r\end{aligned} \tag{12}$$

With discrete input-output curve data for the pumping mode from Ludington PSH station, we can calculate $\min_{v^{(1)}_r, v^{(2)}_r \in [\underline{V}_r, \overline{V}_r], v^{(1)}_r < v^{(2)}_r}$ LHS of (12) $=$ 228.8 hours, which is significantly grater than 6 hours, the maximum RHS of (12) for $\Delta t = 1$ hour. In this case, the number of units that share this reservoir can be up to 228 without breaking the condition. Moreover, a smaller time interval Δt in the optimization model would make *Condition 2* more solid.

III. Disjunctive Convex Hull Model and ACD based Input-output Curve Partition

The hypograph relaxation of an input-output curve is proved to be exact in terms of the objective value, and can be recovered to an exact solution (if applicable) for PSH under given conditions. As convexity is not necessarily required in the hypograph relaxation approach, the hypograph is approximated for non-convex input-output curves through a disjunctive convex hull modeling. The detailed formulation and ACD based partition algorithms are offered in this section.

A. Disjunctive Convex Hull

1) Constraints for the Generating Mode: Given a partition on the (q^{g}_h, v_r) plane, the input-output curve can be divided into multiple components. These components are approximated by their convex hull within acceptable tolerance. Then the hypograph for the generating mode in (5a) is constructed by the union of all the convex hulls, as shown in (13). The convex hull for each component i is modeled in (13a). Equation (13b) guarantees no more than one component is selected. A binary-coded mapping between the binary variables $\zeta^{\mathrm{g}}_{h,t,\ell}$ and the selection variables $\phi^{\mathrm{g}}_{h,t,i}$ is established in (13c). Note $\phi^{\mathrm{g}}_{h,t,i}$ are defined as continuous variables. By summing up of the ancillary variables in all components, the generating power and flow rate are obtained, as shown in (13d) and (13e), respectively. Binary variables are declared in (13f).

$$\gamma^{\mathrm{pg}}_{h,i,k}p^{\mathrm{g}}_{h,t,i} + \gamma^{\mathrm{qg}}_{h,i,k}q^{\mathrm{g}}_{h,t,i} + \gamma^{\mathrm{vg}}_{h,i,k}v^{\mathrm{g}}_{h,t-1,i} \leq \gamma^{0}_{h,i,k}\phi^{\mathrm{g}}_{h,t,i} \quad \forall h\in\mathcal{H}_r,\ \forall t\in\mathcal{T},\ \forall i\in\mathcal{I}^{\mathrm{g}}_h,\ \forall k\in\mathcal{K}_i \tag{13a}$$

$$\sum\nolimits_{i\in\mathcal{I}^{\mathrm{g}}_h}\phi^{\mathrm{g}}_{h,t,i} = u^{\mathrm{g}}_{h,t} \quad \forall h\in\mathcal{H}_r,\ \forall t\in\mathcal{T} \tag{13b}$$

$$\sum\nolimits_{\tilde{i}\in\{\tilde{i}:\tilde{i}\in\mathcal{I}^{\mathrm{g}}_h,\tilde{i}\neq i\}}\phi^{\mathrm{g}}_{h,t,\tilde{i}} \leq \sum\nolimits_{\ell\in\{\ell:B_{i,\ell}=0\}}\zeta^{\mathrm{g}}_{h,t,\ell} + \sum\nolimits_{\ell\in\{\ell:B_{i,\ell}=1\}}(1-\zeta^{\mathrm{g}}_{h,t,\ell}) \quad \forall h\in\mathcal{H}_r,\ \forall t\in\mathcal{T},\ \forall i\in\mathcal{I}^{\mathrm{g}}_h \tag{13c}$$

$$p^{\mathrm{g}}_{h,t} = \sum\nolimits_{i\in\mathcal{I}^{\mathrm{g}}_h}p^{\mathrm{g}}_{h,t,i} \quad \forall h\in\mathcal{H}_r,\ \forall t\in\mathcal{T} \tag{13d}$$

$$q^{\mathrm{g}}_{h,t} = \sum\nolimits_{i\in\mathcal{I}^{\mathrm{g}}_h}q^{\mathrm{g}}_{h,t,i} \quad \forall h\in\mathcal{H}_r,\ \forall t\in\mathcal{T} \tag{13e}$$

$$\zeta^{\mathrm{g}}_{h,t,\ell}\in\{0,1\} \quad \forall h\in\mathcal{H}_r,\ \forall t\in\mathcal{T},\ \forall \ell\in\mathcal{L}^{\mathrm{g}}_h \tag{13f}$$

2) Constraints for the Pumping Mode: Analogously, the hypograph for the pumping mode in (5b) is constructed by (14). Note for fixed-speed PSH, as the pumping power is fixed, the flow rate is only related to the volume of water in the upper reservoir. Thus, (14) is a two-dimensional formulation.

$$\tau^{\mathrm{qp}}_{h,i,k} q^{\mathrm{p}}_{h,t,i} + \tau^{\mathrm{vp}}_{h,i,k} v^{\mathrm{p}}_{h,t-1,i} \le \tau^{0}_{h,i,k} \phi^{\mathrm{p}}_{h,t,i} \quad \forall h \in \mathcal{H}_r,\ \forall t \in \mathcal{T},\ \forall i \in \mathcal{I}^{\mathrm{p}}_h,\ \forall k \in \mathcal{K}_i \text{ (14a)}$$

$$\sum\nolimits_{i \in \mathcal{I}^{\mathrm{p}}_h} \phi^{\mathrm{p}}_{h,t,i} = u^{\mathrm{p}}_{h,t} \quad \forall h \in \mathcal{H}_r,\ \forall t \in \mathcal{T} \text{ (14b)}$$

$$\sum\nolimits_{\tilde{i} \in \{\tilde{i}: \tilde{i} \in \mathcal{I}^{\mathrm{p}}_h, \tilde{i} \neq i\}} \phi^{\mathrm{p}}_{h,t,\tilde{i}} \le \sum\nolimits_{\ell \in \{\ell: B_{i,\ell}=0\}} \zeta^{\mathrm{p}}_{h,t,\ell} + \sum\nolimits_{\ell \in \{\ell: B_{i,\ell}=1\}} (1 - \zeta^{\mathrm{p}}_{h,t,\ell}) \quad \forall h \in \mathcal{H}_r,\ \forall t \in \mathcal{T},\ \forall i \in \mathcal{I}^{\mathrm{p}}_h \text{ (14c)}$$

$$q^{\mathrm{p}}_{h,t} = \sum\nolimits_{i \in \mathcal{I}^{\mathrm{p}}_h} q^{\mathrm{p}}_{h,t,i} \quad \forall h \in \mathcal{H}_r,\ \forall t \in \mathcal{T} \text{ (14d)}$$

$$\zeta^{\mathrm{p}}_{h,t,\ell} \in \{0,1\} \quad \forall h \in \mathcal{H}_r,\ \forall t \in \mathcal{T},\ \forall \ell \in \mathcal{L}^{\mathrm{p}}_h \text{ (14e)}$$

3) Other Constraints: As the modeling for pumping, generating, and idle modes share the same upper reservoir volume variable, by summing up volume variables that are related to all the components, we have an equation to calculate the volume, as shown in (15a). Bound constraints for volume variable that corresponds to the idle-mode component are presented in (15b).

$$v_{r,t} = \sum\nolimits_{i \in \mathcal{I}^{\mathrm{g}}_h} v^{\mathrm{g}}_{h,t,i} + \sum\nolimits_{i \in \mathcal{I}^{\mathrm{p}}_h} v^{\mathrm{p}}_{h,t,i} + v^{\mathrm{i}}_{h,t} \quad \forall h \in \mathcal{H}_r,\ \forall t \in \mathcal{T} \text{ (15a)}$$

$$\underline{V}_r \cdot (1 - u^{\mathrm{g}}_{h,t} - u^{\mathrm{p}}_{h,t}) \le v^{\mathrm{i}}_{h,t} \le \overline{V}_r \cdot (1 - u^{\mathrm{g}}_{h,t} - u^{\mathrm{p}}_{h,t}) \quad \forall h \in \mathcal{H}_r,\ \forall t \in \mathcal{T} \text{ (15b)}$$

When the generating mode is off, $\phi^{\mathrm{g}}_{h,t,i} = 0$ holds according to (13b). Then constraints (13c) is always satisfied for any values of $\zeta^{\mathrm{g}}_{h,t,\ell}$. We reduce the number of $\zeta^{\mathrm{g}}_{h,t,\ell}$ combinations in this situation by incorporating (16a). The corresponding constraints for the pumping mode are shown in (16b).

$$\zeta^{\mathrm{g}}_{h,t,\ell} \le u^{\mathrm{g}}_{h,t} \quad \forall h \in \mathcal{H}_r,\ \forall t \in \mathcal{T},\ \forall \ell \in \mathcal{L}^{\mathrm{g}}_h \text{ (16a)}$$

$$\zeta^{\mathrm{p}}_{h,t,\ell} \le u^{\mathrm{p}}_{h,t} \quad \forall h \in \mathcal{H}_r,\ \forall t \in \mathcal{T},\ \forall \ell \in \mathcal{L}^{\mathrm{p}}_h \text{ (16b)}$$

B. ACD based Partition Algorithm: 3-Dimensional

In this subsection, we elaborate on a three-dimensional approximate convex decomposition (ACD) based partition algorithm that is customized for PSH input-output curves. Note subscripts h and t for unit and time indices, respectively, are eliminated for convenience.

1) Dual Graph Construction: For a given mesh M that represents an input-output curve, its dual graph M^* is first generated. Nodes of M^* correspond to faces of M. A link exists for any two nodes in M^* if the respective faces in M share a common edge[2]. Detailed examples can be further found in [26].

[2]To distinguish the terms *vertex*, *edge*, *face* in geometry (e.g., in mesh M), and the terms *vertex*, *edge* in graph (e.g., in dual graph M^*), we use *node* and *link* to represent *vertex* and *edge*, respectively, which are also conventionally used in graph theory. However, we still preserve *edge* in *half-edge collapses* of a graph later in this paper.

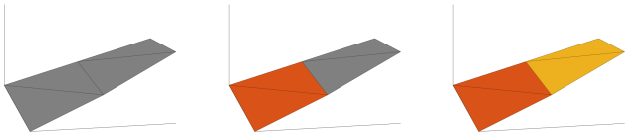

(a) (b) (c)

Fig. 2. A conceptual illustration of the merging process: (a) original mesh, (b) mesh after the first merging, (c) mesh after the second merging

2) Nodes Merge: A sequential merging process is performed until a predefined stopping criterion is reached. In each iteration, we define merge action on link l as a half-edge collapses [29] for nodes $n_1(l)$ and $n_2(l)$ at both ends of l. In detail, nodes $n_1(l)$ and $n_2(l)$ are merged to a new node n_{12}, link l is canceled, and other links that are connected to either $n_1(l)$ or $n_2(l)$ are reconnected to the new merged vertex n_{12}. As an illustrative example, the mesh in Fig. 2a is finally merged to two components as in Fig. 2c under a predefined tolerance, according to the weight of links in the dual graph.

The weight and related metric definitions are important to high quality node-merging choices in each iteration, and the stopping criteria of the algorithm. Three metrics for merge actions are first introduced. With these metrics, weight is then defined for each link in the dual graph.

Shape metric $\mathrm{shp}^{\mathrm{g}}_l$: We first employ the shape metric defined in [26] to guide the generation of compact clusters. As shown in (17a), shape metric $\mathrm{shp}^{\mathrm{g}}_l$ is defined for each link l to assess the cluster compactness after a merge action happens on l.

$$\mathrm{shp}^{\mathrm{g}}_l = \rho_l^2 / (4\pi \cdot \sigma_l) \text{ (17a)}$$

where ρ_l and σ_l are perimeter and area of the mesh M_l, respectively, which can be calculated by assuming a merge action happens on l.

Error metric in generating power $\mathrm{err}^{\mathrm{g}}_l$: In our specific problem, we use new metrics to quantify the performance in terms of convex estimation error. Taking the generating mode as an example, we note our input-output curve is a function in the form of $(q^{\mathrm{g}}, v) \to p^{\mathrm{g}}$, i.e., exact one power generation level p^{g} corresponds to each (q^{g}, v) pair. Thus, different from general three dimensional meshes, a partition on the (q^{g}, v) plane works for our input-output curve. As we mainly concern estimation errors on the p^{g} axis, convex estimation error metric $\mathrm{err}^{\mathrm{g}}_l$ is defined to assess how good the upper convex hull approximation is for a merge action on l. As shown in (17b), $\mathrm{err}^{\mathrm{g}}_l$ is the p^{g}-axis distance between the far most point and the upper convex hull after a merge action happening on l. As an input parameter for the algorithm, $\mathrm{tol}^{\mathrm{g}}$ represents estimation error threshold. Given this, $\mathrm{err}^{\mathrm{g}}_l \le \mathrm{tol}^{\mathrm{g}}$ should be guaranteed for a merge action on l.

$$\mathrm{err}^{\mathrm{g}}_l = \max_{j \in \mathcal{J}_l} \Big[\min_{k \in \mathcal{K}^{\mathrm{upper}}_l} \left(\gamma^{0}_{l,k} - \gamma^{\mathrm{qg}}_{l,k} \hat{q}^{\mathrm{g}(j)} - \gamma^{\mathrm{vg}}_{l,k} \hat{v}^{\mathrm{g}(j)} \right) \Big/ \gamma^{\mathrm{pg}}_{l,k} - \hat{p}^{\mathrm{g}(j)} \Big] \text{ (17b)}$$

where, $\mathcal{J}_l$ is the set of points $\left(\hat{q}^{\mathrm{g}(j)}, \hat{v}^{\mathrm{g}(j)}, \hat{p}^{\mathrm{g}(j)}\right)$ for the mesh M_l obtained from the merge action on l. $\mathcal{K}^{\mathrm{upper}}_l$ is the set of

linear inequality constraints in upper convex hull of the mesh M_l. Note $\gamma^{\text{pg}}_{l,k}$ is nonzero for constraints in upper convex hull $\mathcal{K}^{\text{upper}}_l$. Coefficients $\gamma^{0}_{l,k}$, $\gamma^{\text{pg}}_{l,k}$, $\gamma^{\text{qg}}_{l,k}$, and $\gamma^{\text{vg}}_{l,k}$ are defined in a similar manner to that in (13a).

Error metric in (q^{g}, v) plane cav^{g}_l: In addition, to avoid large errors on feasible region description in the (q^{g}, v) plane, a concavity metric cav^{g}_l is defined in (17c) for a merge action on l, which measures how far it is between the boundary of projected mesh and its convex hull. Given a tolerance $\text{tol}^{\text{cav g}}$ for concavity in the (q^{g}, v) plane, $\text{cav}^{\text{g}}_l \leq \text{tol}^{\text{cav g}}$ is taken as a hard requirement in the merging process.

$$\text{cav}^{\text{g}}_l = \max_{j \in \{j \in \mathcal{J}_l | (\hat{q}^{\text{g}(j)}, \hat{v}^{\text{g}(j)}) \in \mathcal{B}_l\}} \text{dist}\left((\hat{q}^{\text{g}(j)}, \hat{v}^{\text{g}(j)}), \mathcal{B}^{\text{conv}}_l\right) \quad (17c)$$

where, by defining $\text{proj}_{\text{qv}}(\cdot)$ as an orthogonal projection of a three-dimensional mesh into the (q^{g}, v) plane, we denote the boundary of projected M_l as $\mathcal{B}_l$ in (17d). The the convex hull boundary of projected points are defined as $\mathcal{B}^{\text{conv}}_l$ in (17e). $\text{dist}\left((\hat{q}^{\text{g}(j)}, \hat{v}^{\text{g}(j)}), \mathcal{B}^{\text{conv}}_l\right)$ is the minimum Euclidean distance from point $(\hat{q}^{\text{g}(j)}, \hat{v}^{\text{g}(j)})$ to convex hull boundary $\mathcal{B}^{\text{conv}}_l$.

$$\mathcal{B}_l = \partial\ \text{proj}_{\text{qv}}(M_l) \quad (17d)$$

$$\mathcal{B}^{\text{conv}}_l = \partial\ \text{conv}\left(\left\{(\hat{q}^{\text{g}(j)}, \hat{v}^{\text{g}(j)}) \mid j \in \mathcal{J}_l\right\}\right) \quad (17e)$$

Weight definition: Considering these metrics, a weight w^{g}_l to finally evaluate the performance for the merge action on l is defined in (18a). To avoid merge actions that may cause predefined thresholds exceeded, in comparison to the weight in [26], we add two indicator-function terms to the weight definition. The indicator function [30, p. 218] $\text{ind}(\cdot)$, as defined in (18c), can be understood as a penalty defined to avoid violating user-defined tolerance. The choice of α in (18b) ensures the shape term is significantly less than the estimation-error term for disk-shaped meshes at the late stage of the algorithm [26].

$$\begin{aligned} w^{\text{g}}_l = {} & \text{err}^{\text{g}}_l + \alpha \cdot \text{shp}^{\text{g}}_l \\ & + \text{ind}(\text{err}^{\text{g}}_l \leq \text{tol}^{\text{g}}) + \text{ind}(\text{cav}^{\text{g}}_l \leq \text{tol}^{\text{cav g}}) \end{aligned} \quad (18a)$$

where,

$$\alpha = \text{tol}^{\text{g}}/10 \quad (18b)$$

$$\text{ind}(\text{condition}) = \begin{cases} 0 & \text{if condition is satisfied} \\ +\inf & \text{otherwise} \end{cases} \quad (18c)$$

3) The Whole Algorithm: Finally, the whole three-dimensional algorithm is summarized in Algorithm 1. After obtaining the final dual graph from this algorithm, hyperplane constraints are generated for convex hull in each node by using the on-the-shelf tool in [31].

Algorithm 1: ACD_3dim(M, tol^{g}, $\text{tol}^{\text{cav g}}$)

```
Initialize iteration counter n_iter ← 1;
Generate dual graph M* for a given mesh M;
while min_l w^g_l < +inf do
    Find the link l̂ with smallest weight w^g_l̂;
    Perform half-edge collapses on the nodes at
     two-ends of l̂;
    n_iter ← n_iter + 1;
    Update weight metric w^g_l by using (18a);
end
```

Algorithm 2: ACD_2dim(P, tol^{p})

```
if err^p(P) < tol^p then
    Add P to the component list, and return;
else
    Find point j* that has maximum distance in (19);
    P_1 ← {(q̂^p(j), v̂^p(j)) ∈ P, q̂^p(j) ≤ q̂^p(j*)};
    P_2 ← {(q̂^p(j), v̂^p(j)) ∈ P, q̂^p(j) ≥ q̂^p(j*)};
    for i = 1 to 2 do
        ACD_2dim(P_i, tol^p);
    end
end
```

C. ACD based Partition Algorithm: 2-Dimensional

For the pumping mode of fixed-speed PSH, input-output curves need a two-dimensional partition algorithm. In contrast to employing a merge-based algorithm for three-dimensional cases, we use a divide-and-conquer strategy in [24], as its performance is guaranteed theoretically according to [24]. In our application, analogous to err^{g} for the generating mode, a convex approximation error metric err^{p} for the pumping mode is defined in (19), which is the maximum distance between points and the convex hull in the q^{p}-axis.

$$\text{err}^{\text{p}}_i = \max_{j \in \mathcal{J}_i} \left[\min_{k \in \mathcal{K}^{\text{upper}}_i} \left(\tau^{0}_{i,k} - \tau^{\text{vp}}_{i,k} \hat{v}^{\text{p}(j)}\right) \Big/ \tau^{\text{qp}}_{i,k} - \hat{q}^{\text{p}(j)} \right] \quad (19)$$

where, $\mathcal{J}_i$ is the set of nodes $\left(\hat{q}^{\text{p}(j)}, \hat{v}^{\text{p}(j)}\right)$ of i-th polygon. $\mathcal{K}^{\text{upper}}_i$ is the set of linear inequality constraints in upper convex hull of i-th polygon. Coefficients $\tau^{0}_{i,k}$, $\tau^{\text{qp}}_{i,k}$, and $\tau^{\text{vp}}_{i,k}$ are defined in a similar manner to that in (14a).

The algorithm is defined recursively as shown in Algorithm 2, which keeps dividing polygons until the tolerance criterion is satisfied. As the pumping input-output curve is a function of one variable, the division strategy could be simplified in comparison to the version in [24]. We divide a polygon with inequalities $q^{\text{p}} \leq \hat{q}^{\text{p}(j^*)}$ and $q^{\text{p}} \geq \hat{q}^{\text{p}(j^*)}$, where j^* is the index for point that has maximum distance in (19). In our implementation, hyperplane constraints are generated by using tool in [31].

IV. A Case Study of the Ludington PSH Plant

We tested our proposed approach by using a real-world Ludington PSH station case, in which the PSH profit maximization problem is addressed to assess the relaxation exactness and other numerical performances of our proposed approach. All the MILP problems were built with YALMIP [32] and solved by Gurobi solver 9.0.3 [33] on a computer with Intel Core i7-9700 CPU and 64 GB RAM.

A. Case Settings

Located in Michigan, the Ludington PSH power plant is the fifth largest PSH station in the world in terms of installed

TABLE I
PARAMETERS FOR LUDINGTON PSH UNITS AND UPPER RESERVOIR

$\overline{P}^{\mathrm{g}}$	$\underline{P}^{\mathrm{g}}$	$\overline{P}^{\mathrm{p}} = \underline{P}^{\mathrm{p}}$	$\overline{V}$
398 MW	250 MW	362 MW	56935 ac ft
$\overline{Q}^{\mathrm{g}}$	$\underline{Q}^{\mathrm{g}}$	$\overline{Q}^{\mathrm{p}}$	$\underline{Q}^{\mathrm{p}}$
15385 $\mathrm{ft}^3{\cdot}\mathrm{s}^{-1}$	9488 $\mathrm{ft}^3{\cdot}\mathrm{s}^{-1}$	13572 $\mathrm{ft}^3{\cdot}\mathrm{s}^{-1}$	11484 $\mathrm{ft}^3{\cdot}\mathrm{s}^{-1}$

power capacity [34]. It has an upper reservoir with 82,860 ac ft total capacity (which includes non-active capacity), a lower reservoir of Lake Michigan, and six PSH units. For each PSH unit, a Francis pump turbine with 362 MW installed capacity is equipped. We use realistic data for Ludington PSH units in our numerical experiments to test our proposed approach. The six units in Ludington PSH power plant are assumed to have identical parameters, which are listed in Table I. As shown in Fig. 3, the input-output curves of PSH units, which were obtained by fitting field test data, indicate variable energy conversion efficiencies at different operating points. Moreover, we note the maximum power bound also increases as the water volume in the upper reservoir increases. Thus, the characters of both variable efficiency and head-dependent power bound are considered in our input-output curve modeling.

In our numerical tests, day-head profit maximization problems from the PSH owners' perspective were solved by using the proposed relaxed formulation in (7). The optimization horizon is 24 hours, and the resolution is 1 hour. Historical LMP profiles from MISO day-ahead market [35] are used in our tests. The gaps for the MILP problems are set as 0.5%.

B. Relaxation Exactness

The input-output curve is modeled using our proposed disjunctive convex hull formulation with ACD-based partition method. As shown in Fig. 3b, for tolerance $\mathrm{tol}^{\mathrm{g}} = 2.5$, the generating-mode input-output curve is divided by four blocks, and the curve corresponding to each block is modeled by a convex hull. In Fig. 3c, as the input-output curve for the pumping mode is close to a convex curve, it is modeled using only one convex hull block.

In the case with a tolerance $\mathrm{tol}^{\mathrm{g}} = 2.5$ and a typical LMP profile, an optimal solution and the convex hull approximation are shown in Fig. 3b, in which the red stars represent the optimal solution. As indicated, since all red stars fall on the blockwise-convexified input-output curve, the proposed disjunctive convex hull model is an exact relaxation for the curve in this test, which is checked numerically in the following.

Given an optimal solution, for each unit h and each time period t, relaxation exactness indices are defined to check if the relaxation is exact, in (20a) and (20b) for generating and pumping modes, respectively. Taking the generating mode as an example, as the optimal solution is a feasible solution, the difference between RHS and LHS of (13a) is non-negative, thus, $\mathrm{REI}^{\mathrm{g}}_{h,t} \geq 0$. If the inequality in (13a) holds with equality for any plane in the upper convex hull of $\mathcal{K}^{\mathrm{upper}}_{\tilde{i}_{h,t}}$, which means the optimal solution falls on the upper convex hull, we have $\mathrm{REI}^{\mathrm{g}}_{h,t} = 0$. The same rule applies to the pumping mode. Consequently, the condition $\sum_{\forall h \in \mathcal{H}_r, \forall t \in \mathcal{T}} (\mathrm{REI}^{\mathrm{g}}_{h,t} + \mathrm{REI}^{\mathrm{p}}_{h,t}) = 0$ can be used for a plant to identify if a given optimal solution falls on the upper convex hull. In our test case, this condition is satisfied under 10^{-8} level numerical tolerance, thus the relaxation is exact. The case shown in Fig. 3 is used for illustration purposes. We also check all the cases shown later in Tables III and IV, and the relaxations are all exact.

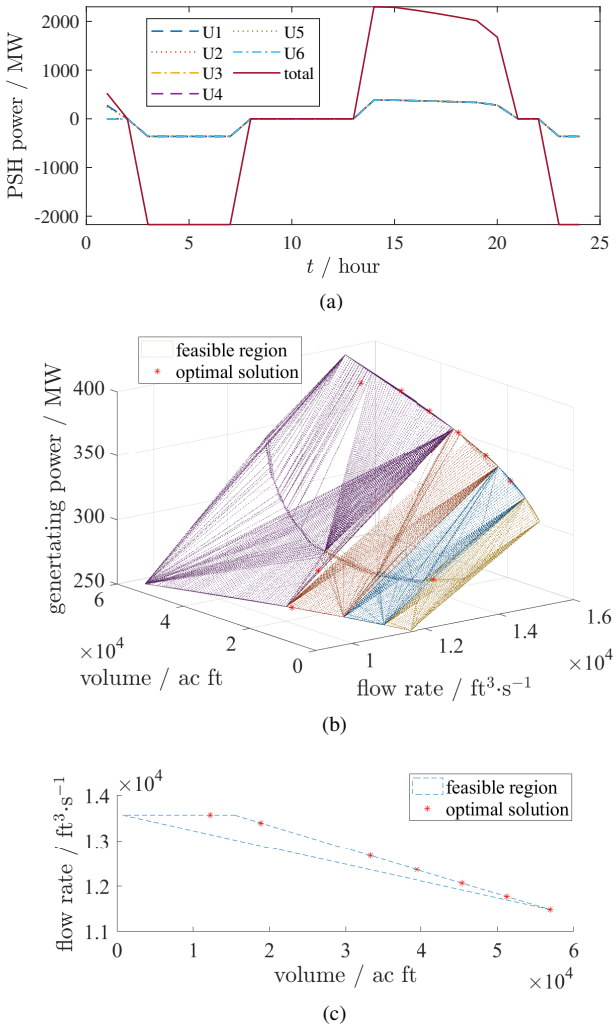

Fig. 3. Solution for PSH owners' profit maximization problems: (a) dispatch of PSH plant, (b) solution for the generating mode, and (c) solution for the pumping mode. Overlaps occur in sub-figure (a).

$$\mathrm{REI}^{\mathrm{g}}_{h,t} = \min_{\forall k \in \mathcal{K}^{\mathrm{upper}}_{\tilde{i}_{h,t}}} \Big[\Big(\gamma^{0}_{h,\tilde{i}_{h,t},k} - \gamma^{\mathrm{qg}}_{h,\tilde{i}_{h,t},k} q^{\mathrm{g}*}_{h,t,\tilde{i}_{h,t}} - \gamma^{\mathrm{vg}}_{h,\tilde{i}_{h,t},k} v^{\mathrm{g}*}_{h,t-1,\tilde{i}_{h,t}} \Big) \Big/ \gamma^{\mathrm{pg}}_{h,\tilde{i}_{h,t},k} - p^{\mathrm{g}*}_{h,t,\tilde{i}_{h,t}} \Big] \quad \forall h \in \mathcal{H}_r,\ \forall t \in \mathcal{T} \tag{20a}$$

$$\mathrm{REI}^{\mathrm{p}}_{h,t} = \min_{\forall k \in \mathcal{K}^{\mathrm{upper}}_{\hat{i}_{h,t}}} \Big[\Big(\tau^{0}_{h,\hat{i}_{h,t},k} - \tau^{\mathrm{vp}}_{h,\hat{i}_{h,t},k} v^{\mathrm{p}*}_{h,t-1,\hat{i}_{h,t}} \Big) \Big/ \tau^{\mathrm{qp}}_{h,\hat{i}_{h,t},k} - q^{\mathrm{p}*}_{h,t,\hat{i}_{h,t}} \Big] \quad \forall h \in \mathcal{H}_r,\ \forall t \in \mathcal{T} \tag{20b}$$

where, $\tilde{i}_{h,t}$ in (20a) and $\hat{i}_{h,t}$ in (20b) are the indices i such that $\phi^{\mathrm{g}}_{h,t,i} = 1$ and $\phi^{\mathrm{p}}_{h,t,i} = 1$, respectively.

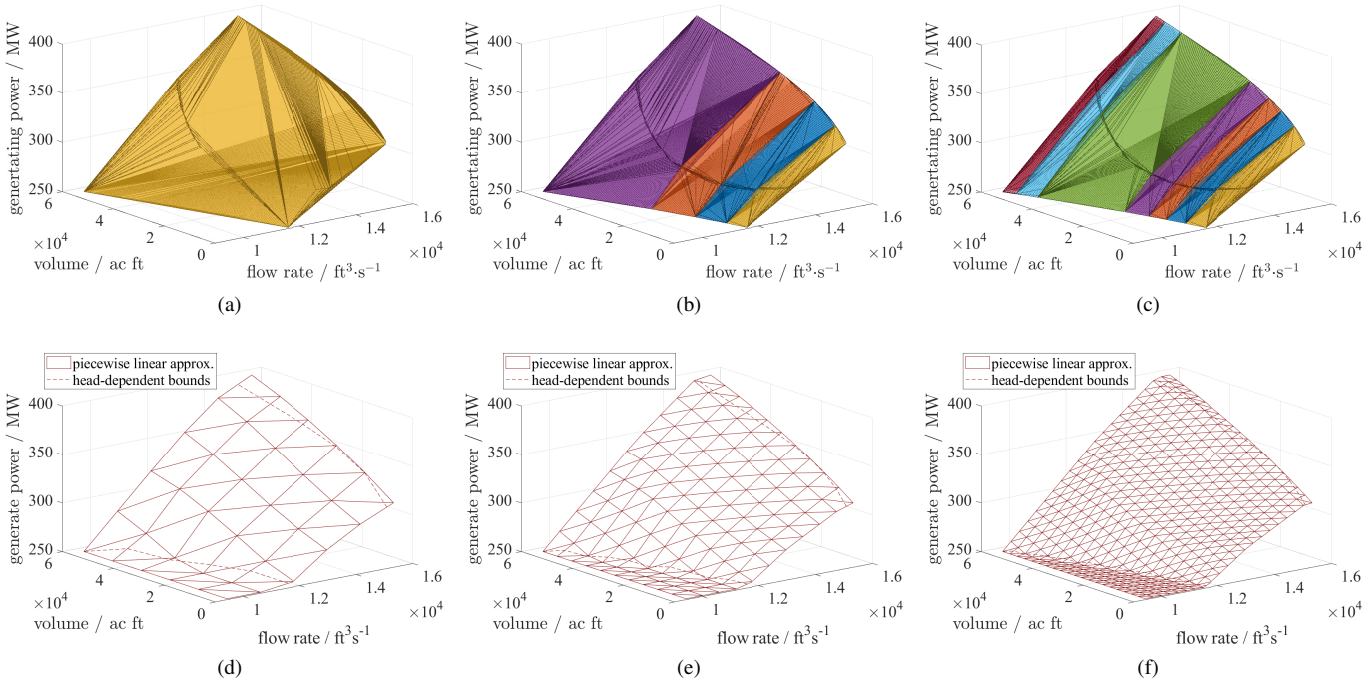

Fig. 4. Input-output curve modeling methods: sub-figures (a), (b), and (c) are disjunctive convex modeling for $\text{tol}^{\text{g}} = 10, 2.5, 1.5$, respectively; sub-figures (d), (e), and (f) are piece-wise linear modeling for $n = 5, 10, 20$, respectively

TABLE II
MILP PROBLEM SIZE COMPARISON

model	# of variables			# of constraints	
	integer[1]	binary	continuous	equality	inequality
DCH $\text{tol}^{\text{g}} = 10$ (CH)[1]	0	288	2064	1200	72326
DCH $\text{tol}^{\text{g}} = 2.5$	0	576	3792	1200	88886
DCH $\text{tol}^{\text{g}} = 1.5$	0	720	5520	1200	99830
PWL $n = 5$ [2]	864	864	8688	1200	13430
PWL $n = 10$	1152	864	23088	1200	28406
PWL $n = 20$	1440	864	73488	1200	79382

[1] Here "integer" represents the number of general integer variables, which does not include the number of binary variables.
[2] The input parameter $\text{tol}^{\text{g}} = 10$ is larger than the resultant maximum error 5.878. Thus, only one component (i.e., the convex hull) is finally obtained. It is equivalent to a CH method.
[3] For PWL method, $n = 5$ means 5×5-pieces for the generating input-output curve. The same applies for $n = 10$ and $n = 20$ cases.

TABLE III
SOLUTION TIME COMPARISON UNDER DIFFERENT LMP PROFILES

model	time under LMPs (s)			
	LMP 1	LMP 2	LMP 3	LMP 4
DCH $\text{tol}^{\text{g}} = 10$ (CH)	240.6	163.5	59.5	159.0
DCH $\text{tol}^{\text{g}} = 2.5$	1083.3	1159.3	110.8	383.4
DCH $\text{tol}^{\text{g}} = 1.5$	1237.8	1684.9	227.4	554.7
PWL $n = 5$	> 7200	> 7200	1782.3	972.1
PWL $n = 10$	> 7200	> 7200	4558.5	965.7
PWL $n = 20$	> 7200	> 7200	> 7200	> 7200
model	LMP 5	LMP 6	LMP 7	LMP 8
DCH $\text{tol}^{\text{g}} = 10$ (CH)	67.5	8.5	127.6	148.2
DCH $\text{tol}^{\text{g}} = 2.5$	514.6	287.1	611.3	843.0
DCH $\text{tol}^{\text{g}} = 1.5$	1679.0	658.6	2094.3	1567.6
PWL $n = 5$	> 7200	> 7200	> 7200	4706.7
PWL $n = 10$	> 7200	> 7200	> 7200	> 7200
PWL $n = 20$	> 7200	> 7200	> 7200	> 7200

C. Performance Comparison

To facilitate a numerical performance comparison, the input-output curve is approximated by three methods: piece-wise linear approximation method (PWL), convex hull approximation method (CH), and the proposed disjunctive convex hull approximation method (DCH). PWL method is implemented by a zig-zag integer formulation [20]. The detailed implementation for the ZZI formulation is provided in the supplementary material [36]. In Fig. 4, sub-figures (a), (b), and (c) show how our proposed disjunctive convex hull approach models the input-output curve under different tolerance settings; while sub-figures (d), (e), and (f) illustrate the piece-wise linear modeling under different number of pieces. Note given a large enough tol^{g}, our partition method would come out with only one component, which is equivalent to the traditional CH approximation method. As shown in Fig. 4a, DCH approach with $\text{tol}^{\text{g}} = 10$ in this case study has only one component, thus it can be treated as a CH method implementation.

We tested eight daily cases with distinctive LMP settings. The detailed data can be found in the supplementary material [36]. Table II shows a comparison of MILP problem size for different methods. Given only input parameters differ in these cases, the problem size for the eight cases are the same. As indicated, different case settings, such as the number of pieces in PWL and the tolerance in CH, affect the number of general-integer and binary variables. The PWL method with ZZI formulation has more general-integer and binary variables than the DCH method. As a result, in Table III, most of the PWL cases didn't converge in 2 hours even for those 5×5-piece cases. The solution time of DCH cases increases as the

TABLE IV
SENSITIVITY ANALYSIS FOR INITIAL AVAILABLE VOLUME PERCENTAGES OF THE UPPER RESERVOIR (WITH LMP 7)

model	time under initial available volumes in percentage (s)				
	25%	37.5%	50%	62.5%	75%
DCH $\text{tol}^{\text{g}} = 10$ (CH)	126.6	169.3	127.6	134.9	153.9
DCH $\text{tol}^{\text{g}} = 2.5$	1464.3	2287.8	611.3	2875.5	1644.1
DCH $\text{tol}^{\text{g}} = 1.5$	3399.0	> 7200[1]	2094.3	6048.4	5533.4
PWL $n = 5$	> 7200	> 7200	> 7200	> 7200	> 7200
PWL $n = 10$	> 7200	> 7200	> 7200	> 7200	> 7200
PWL $n = 20$	> 7200	> 7200	> 7200	> 7200	> 7200

[1] Although this case doesn't converge to 0.5% gap, an obtained feasible solution with 0.54% gap is also acceptable to use. For the same case, the PWL models offer solutions with 1.93%, 2.53%, and 5.16% gaps for 5×5, 10×10, and 20×20-piece settings, respectively.

tolerance tol^{g} decreases. Compared with the PWL method, our DCH approach can enable solution time accelerations under the same LMP setting. Sensitivity analysis for various initial volume levels is also conducted with LMP 7, which is the most time consuming case in Table III. We define initial available volume in percentage as $(v_{r,0} - \underline{V}_r) / (\overline{V}_r - \underline{V}_r)$ to represent the initial volume status in the upper reservoir. Results shown in Table IV also verify the advantage of our approach in solution time.

To assess the approximation accuracy, we estimate the empirical cumulative distribution function (CDF) of modeling error for the generating input-output curve based on uniform sampling in the (q^{g}, v) space. Fig. 5 shows a comparison of empirical CDFs for CH, DCH, and PWL methods. As indicated, DCH cases with $\text{tol}^{\text{g}} = 2.5$ or 1.5 introduce less estimation error than the CH case does. A summary of maximum estimation errors for these methods is shown in Table V. As indicated, the estimation error for both DCH and PWL methods can be reduced with larger tolerance and a larger number of pieces, respectively. The CH approach, i.e. DCH approach with $\text{tol}^{\text{g}} = 10$, has a relatively large error. Taking the solution time into account, the PWL method didn't converge in 2 hours even for most 5×5-piece cases, as

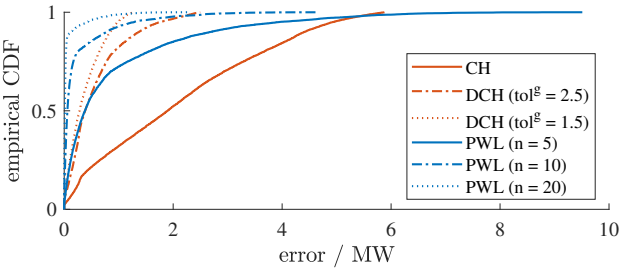

Fig. 5. Empirical CDF Comparison

TABLE V
MAXIMUM APPROXIMATION ERROR COMPARISON

DCH			PWL	
tol^{g}	# of comp.	max error (MW)	n	max error (MW)
10 (CH) *	1	5.878	5	9.510
2.5	4	2.496	10	4.625
1.5	7	1.267	20	2.296

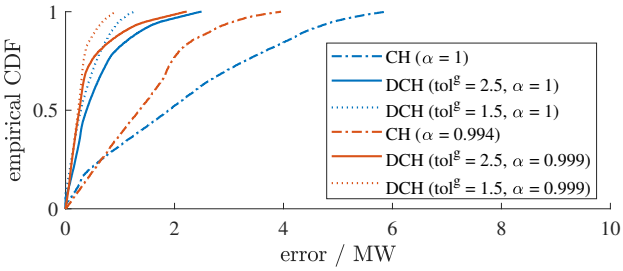

Fig. 6. Effect of optimal regression term α on empirical CDF

shown in Table III. Our proposed DCH method has better performance in solution time than the PWL method under similar estimation error settings.

Both the DCH and CH methods can incorporate the regression term proposed in [21] to adjust their estimation errors, in which optimal regression term α can be obtained by using optimization techniques. The regression term α is selected in a range of $(0, 1]$, specially, case with $\alpha = 1$ is equivalent to that without incorporating regression term (see [21] for detail). We use an enumeration method with resolution 0.001 for α to find the optimal α values for the DCH and CH cases. The performance comparison is shown in Fig. 6. Overall, the regression term in [21] can improve the performance of both CH and DCH methods. The CH method under optimal regression term can not outperform the DCH method ($\text{tol}^{\text{g}} = 2.5$ or 1.5) without regression terms.

V. CONCLUSION

This paper proposes a disjunctive convex hull model to approximate the input-output curves for PSH units. Under our proposed sufficient conditions, the exactness of hypograph relaxation on PSH input-output model is theoretically proved and numerically verified. Through numerical tests on a real-world PSH plant, the proposed method is shown to achieve an acceptable estimation error in comparison to the conventional convex hull approach, and significantly shorter solution time in comparison to the piece-wise linear approach. Accurate input-output curve modeling would potentially encounter significant computational challenges for large-scale electricity market applications from ISOs' perspective. Methodologies to address it can be further explored. The proposed sufficient conditions can be further verified if data for more PSH plants is available.

APPENDIX: PROOF OF THE ASSERTION IN (11)

Now we prove the assertion in (11) by using mathematical induction.

For $t = 0$, given $v^{**}_{r,t} = v^{*}_{r,t} = v_{r,0}$, the assertion in (11) is satisfied.

For $1 \le t \le N_t$, if $v^{**}_{r,t-1} \ge v^{*}_{r,t-1}$ holds, we need to prove $v^{**}_{r,t} \ge v^{*}_{r,t}$.

For units with $u^{\text{g}*}_{h,t} = 1$, given $p^{\text{g}*}_{h,t} \le \varphi^{\text{g}}_h(q^{\text{g}*}_{h,t}, v^{*}_{r,t-1})$, $p^{\text{g}**}_{h,t} = \varphi^{\text{g}}_h(q^{\text{g}**}_{h,t}, v^{**}_{r,t-1})$, and $p^{\text{g}**}_{h,t} = p^{\text{g}*}_{h,t}$, we have $\varphi^{\text{g}}_h(q^{\text{g}**}_{h,t}, v^{**}_{r,t-1}) \le \varphi^{\text{g}}_h(q^{\text{g}*}_{h,t}, v^{*}_{r,t-1})$. Moreover, we can get $\varphi^{\text{g}}_h(q^{\text{g}*}_{h,t}, v^{*}_{r,t-1}) \le \varphi^{\text{g}}_h(q^{\text{g}*}_{h,t}, v^{**}_{r,t-1})$ from that $\varphi^{\text{g}}_h(q^{\text{g}}_h, v_r)$ is monotonically non-decreasing on v_r in *Condition 1*. Thus, we

have $\varphi_h^{\mathrm{g}}(q_{h,t}^{\mathrm{g}**}, v_{r,t-1}^{**}) \le \varphi_h^{\mathrm{g}}(q_{h,t}^{\mathrm{g}*}, v_{r,t-1}^{**})$. This further leads to (A-1), under the condition $\varphi_h^{\mathrm{g}}(q_h^{\mathrm{g}}, v_r)$ is monotonically non-decreasing on q_h^{g}, as well as the fact $q_{h,t}^{\mathrm{g}**}$ is the smallest value obtained from $p_{h,t}^{\mathrm{g}**} = \varphi_h^{\mathrm{g}}(q_{h,t}^{\mathrm{g}}, v_{r,t-1}^{**})$ in Step 2. For units with $u_{h,t}^{\mathrm{g}*} = 0$, (A-1) is trivially satisfied.

$$q_{h,t}^{\mathrm{g}**} \le q_{h,t}^{\mathrm{g}*} \tag{A-1}$$

Note $\sum_{h\in\mathcal{H}_r}\left[\varphi_h^{\mathrm{p}}(v_r^{(1)}) - \varphi_h^{\mathrm{p}}(v_r^{(2)})\right]\cdot\Delta t \le v_r^{(2)} - v_r^{(1)}$ in *Condition 2* can be extended from $v_r^{(1)} < v_r^{(2)}$ to $v_r^{(1)} \le v_r^{(2)}$, as it trivially holds for $v_r^{(1)} = v_r^{(2)}$. Let $v_r^{(1)} = v_{r,t-1}^{*}$ and $v_r^{(2)} = v_{r,t-1}^{**}$, we can get (A-2a).

$$v_{r,t-1}^{**} - v_{r,t-1}^{*} \ge \sum\nolimits_{h\in\mathcal{H}_r}\left(\varphi_h^{\mathrm{p}}(v_{r,t-1}^{*}) - \varphi_h^{\mathrm{p}}(v_{r,t-1}^{**})\right)\cdot\Delta t \tag{A-2a}$$

For units with $u_{h,t}^{\mathrm{p}*} = 1$, given $q_{h,t}^{\mathrm{p}*} \le \varphi_h^{\mathrm{p}}(v_{r,t-1}^{*})$, and $q_{h,t}^{\mathrm{p}**} = \varphi_h^{\mathrm{p}}(v_{r,t-1}^{**})$ as indicated in Step 3, $\varphi_h^{\mathrm{p}}(v_{r,t-1}^{*}) - \varphi_h^{\mathrm{p}}(v_{r,t-1}^{**}) \ge q_{h,t}^{\mathrm{p}*} - q_{h,t}^{\mathrm{p}**}$. For units with $u_{h,t}^{\mathrm{p}*} = 0$, given $v_{r,t-1}^{**} \ge v_{r,t-1}^{*}$ and the monotonically non-increasing property of $\varphi_h^{\mathrm{p}}(v_r)$, we have $\varphi_h^{\mathrm{p}}(v_{r,t-1}^{*}) \ge \varphi_h^{\mathrm{p}}(v_{r,t-1}^{**})$. Thus, $\varphi_h^{\mathrm{p}}(v_{r,t-1}^{*}) - \varphi_h^{\mathrm{p}}(v_{r,t-1}^{**}) \ge 0 = q_{h,t}^{\mathrm{p}*} - q_{h,t}^{\mathrm{p}**}$. Consequently, (A-2b) can be further obtained from (A-2a).

$$v_{r,t-1}^{**} \ge v_{r,t-1}^{*} + \sum\nolimits_{h\in\mathcal{H}_r}(q_{h,t}^{\mathrm{p}*} - q_{h,t}^{\mathrm{p}**})\cdot\Delta t \tag{A-2b}$$

From (A-1) and (A-2b), we have,

$$\begin{aligned} v_{r,t}^{**} &= v_{r,t-1}^{**} - \sum\nolimits_{h\in\mathcal{H}_r} q_{h,t}^{\mathrm{g}**}\cdot\Delta t + \sum\nolimits_{h\in\mathcal{H}_r} q_{h,t}^{\mathrm{p}**}\cdot\Delta t \\ &\quad + \hat{q}_{r,t}^{\mathrm{infl}}\cdot\Delta t - \hat{q}_{r,t}^{\mathrm{outfl}}\cdot\Delta t - s_{r,t}^{**} && \text{(A-3a)} \\ &\ge v_{r,t-1}^{*} - \sum\nolimits_{h\in\mathcal{H}_r} q_{h,t}^{\mathrm{g}*}\cdot\Delta t + \sum\nolimits_{h\in\mathcal{H}_r} q_{h,t}^{\mathrm{p}*}\cdot\Delta t \\ &\quad + \hat{q}_{r,t}^{\mathrm{infl}}\cdot\Delta t - \hat{q}_{r,t}^{\mathrm{outfl}}\cdot\Delta t - s_{r,t}^{*} + s_{r,t}^{*} - s_{r,t}^{**} && \text{(A-3b)} \\ &= v_{r,t}^{*} + s_{r,t}^{*} - s_{r,t}^{**} && \text{(A-3c)} \end{aligned}$$

Then we can get $v_{r,t}^{**} + s_{r,t}^{**} \ge v_{r,t}^{*} + s_{r,t}^{*}$. To further compare $v_{r,t}^{**}$ and $v_{r,t}^{*}$, there are two cases to discuss:

- Case 1, $v_{r,t}^{**} + s_{r,t}^{**} \le \overline{V}_r$. From (10), we have $s_{r,t}^{**} = 0$. So, $v_{r,t}^{**} = v_{r,t}^{**} + s_{r,t}^{**} \ge v_{r,t}^{*} + s_{r,t}^{*} \ge v_{r,t}^{*}$.
- Case 2, $v_{r,t}^{**} + s_{r,t}^{**} > \overline{V}_r$. From (10), we have $s_{r,t}^{**} = v_{r,t-1}^{**} - \sum_{h\in\mathcal{H}_r} q_{h,t}^{\mathrm{g}*}\cdot\Delta t + \sum_{h\in\mathcal{H}_r} q_{h,t}^{\mathrm{p}*}\cdot\Delta t + \hat{q}_{r,t}^{\mathrm{infl}}\cdot\Delta t - \hat{q}_{r,t}^{\mathrm{outfl}}\cdot\Delta t - \overline{V}_r$, and $v_{r,t}^{**} = \overline{V}_r$. So, $v_{r,t}^{**} = \overline{V}_r \ge v_{r,t}^{*}$.

Thus, $v_{r,t}^{**} \ge v_{r,t}^{*}$ holds. ∎

ACKNOWLEDGMENT

The authors would like to thank Mike Shi, Kevin J. Van Oirschot, Darrell Newcomer, Karl T. Blaszkowski, and Steven L. Gaarde from Consumers Energy for the data and helpful discussion. We would also like to thank Prof. Ross Baldick, Prof. Lei Wu, as well as anonymous editor and reviewers for their insightful comments.

The views expressed herein do not necessarily represent the views of the U.S. Department of Energy and the United States Government.

REFERENCES

[1] J. Garcia-Gonzalez, R. M. R. de la Muela, L. M. Santos, and A. M. Gonzalez, "Stochastic joint optimization of wind generation and pumped-storage units in an electricity market," *IEEE Transactions on Power Systems*, vol. 23, no. 2, pp. 460–468, 2008.

[2] R. Jiang, J. Wang, and Y. Guan, "Robust unit commitment with wind power and pumped storage hydro," *IEEE Transactions on Power Systems*, vol. 27, no. 2, pp. 800–810, 2011.

[3] K. Bruninx, Y. Dvorkin, E. Delarue, H. Pandžić, W. D haeseleer, and D. S. Kirschen, "Coupling pumped hydro energy storage with unit commitment," *IEEE Transactions on Sustainable Energy*, vol. 7, no. 2, pp. 786–796, 2015.

[4] N. Li and K. W. Hedman, "Enhanced pumped hydro storage utilization using policy functions," *IEEE Transactions on Power Systems*, vol. 32, no. 2, pp. 1089–1102, 2016.

[5] B. Huang, Y. Chen, and R. Baldick, "A configuration based pumped storage hydro model in the miso day-ahead market," *IEEE Transactions on Power Systems*, 2021.

[6] P.-H. Chen, "Pumped-storage scheduling using evolutionary particle swarm optimization," *IEEE Transactions on Energy Conversion*, vol. 23, no. 1, pp. 294–301, 2008.

[7] A. J. Conejo, J. M. Arroyo, J. Contreras, and F. A. Villamor, "Self-scheduling of a hydro producer in a pool-based electricity market," *IEEE Transactions on Power Systems*, vol. 17, no. 4, pp. 1265–1272, 2002.

[8] A. Borghetti, C. D'Ambrosio, A. Lodi, and S. Martello, "An MILP approach for short-term hydro scheduling and unit commitment with head-dependent reservoir," *IEEE Transactions on Power Systems*, vol. 23, no. 3, pp. 1115–1124, 2008.

[9] B. Tong, Q. Zhai, and X. Guan, "An MILP based formulation for short-term hydro generation scheduling with analysis of the linearization effects on solution feasibility," *IEEE Transactions on Power Systems*, vol. 28, no. 4, pp. 3588–3599, 2013.

[10] D. A. Babayev, "Piece-wise linear approximation of functions of two variables," *Journal of Heuristics*, vol. 2, no. 4, pp. 313–320, 1997.

[11] L. Wu, M. Shahidehpour, and Z. Li, "GENCO's risk-constrained hydrothermal scheduling," *IEEE Transactions on Power Systems*, vol. 23, no. 4, pp. 1847–1858, 2008.

[12] B. Brito, E. Finardi, and F. Takigawa, "Mixed-integer nonseparable piecewise linear models for the hydropower production function in the unit commitment problem," *Electric Power Systems Research*, vol. 182, p. 106234, 2020.

[13] J. P. Vielma and G. L. Nemhauser, "Modeling disjunctive constraints with a logarithmic number of binary variables and constraints," *Mathematical Programming*, vol. 128, no. 1-2, pp. 49–72, 2011.

[14] C.-H. Chen, N. Chen, and P. B. Luh, "Head dependence of pump-storage-unit model applied to generation scheduling," *IEEE Transactions on Power Systems*, vol. 32, no. 4, pp. 2869–2877, 2016.

[15] T. Li and M. Shahidehpour, "Price-based unit commitment: A case of lagrangian relaxation versus mixed integer programming," *IEEE transactions on power systems*, vol. 20, no. 4, pp. 2015–2025, 2005.

[16] M. Chazarra, J. I. Pérez-Díaz, and J. García-González, "Optimal energy and reserve scheduling of pumped-storage power plants considering hydraulic short-circuit operation," *IEEE Transactions on Power Systems*, vol. 32, no. 1, pp. 344–353, 2016.

[17] M. Chazarra, J. I. Pérez-Díaz, and J. Garcia-Gonzalez, "Optimal joint energy and secondary regulation reserve hourly scheduling of variable speed pumped storage hydropower plants," *IEEE Transactions on Power Systems*, vol. 33, no. 1, pp. 103–115, 2017.

[18] J. Huchette and J. P. Vielma, "Nonconvex piecewise linear functions: Advanced formulations and simple modeling tools," *Operations Research*, in press.

[19] J. Huchette and J. P. Vielma, "A combinatorial approach for small and strong formulations of disjunctive constraints," *Mathematics of Operations Research*, vol. 44, no. 3, pp. 793–820, 2019.

[20] S. Wang, J. Liu, H. Chen, R. Bo, and Y. Chen, "Modeling state transition and head-dependent efficiency curve for pumped storage hydro in look-ahead dispatch," *IEEE Transactions on Power Systems*, 2021.

[21] A. L. Diniz and M. E. P. Maceira, "A four-dimensional model of hydro generation for the short-term hydrothermal dispatch problem considering head and spillage effects," *IEEE Transactions on Power Systems*, vol. 23, no. 3, pp. 1298–1308, 2008.

[22] T. Pavlidis, "Decomposition of Polygons Into Simpler Components: Feature Generation for Syntactic Pattern Recognition," *IEEE Transactions on Computers*, vol. C-24, no. 6, pp. 636–650, 1975.

[23] B. M. Chazelle, "Convex decompositions of polyhedra," *Proceedings of the Annual ACM Symposium on Theory of Computing*, pp. 70–79, 1981.

[24] J. M. Lien and N. M. Amato, "Approximate convex decomposition of polygons," *Computational Geometry: Theory and Applications*, vol. 35, pp. 100–123, 2006.
[25] J. M. Lien and N. M. Amato, "Approximate convex decomposition of polyhedra and its applications," *Computer Aided Geometric Design*, vol. 25, no. 7, pp. 503–522, 2008.
[26] K. Mamou and F. Ghorbel, "A simple and efficient approach for 3D mesh approximate convex decomposition," *Proceedings - International Conference on Image Processing, ICIP*, pp. 3501–3504, 2009.
[27] Y. Gu, J. Bakke, Z. Zhou, D. Osborn, T. Guo, and R. Bo, "A novel market simulation methodology on hydro storage," *IEEE Transactions on Smart Grid*, vol. 5, no. 2, pp. 1119–1128, 2014.
[28] D. Fernández-Muñoz, J. I. Pérez-Díaz, and M. Chazarra, "A two-stage stochastic optimisation model for the water value calculation in a hybrid diesel/wind/pumped-storage power system," *IET Renewable Power Generation*, vol. 13, no. 12, pp. 2156–2165, 2019.
[29] H. Hoppe, "Progressive meshes," in *Proceedings of the 23rd Annual Conference on Computer Graphics and Interactive Techniques*, 1996, pp. 99–108.
[30] S. Boyd, S. P. Boyd, and L. Vandenberghe, *Convex Optimization*. Cambridge University Press, 2004.
[31] M. Kleder. Vert2con - vertices to constraints, version 1.0.0.0. [Online]. Available: https://www.mathworks.com/matlabcentral/fileexchange/7895-vert2con-vertices-to-constraints
[32] J. Löfberg. YALMIP. [Online]. Available: https://yalmip.github.io/
[33] Gurobi Optimization, LLC. Gurobi optimizer. Beaverton, OR, USA. [Online]. Available: https://www.gurobi.com/products/gurobi-optimizer/
[34] Wikipedia. List of pumped-storage hydroelectric power stations. [Online]. Available: https://en.wikipedia.org/wiki/List_of_pumped-storage_hydroelectric_power_stations
[35] MISO. Market reports. Carmel, IN, USA. [Online]. Available: https://www.misoenergy.org/markets-and-operations/real-time–market-data/market-reports/
[36] S. Wang, J. Liu, R. Bo, and Y. Chen. Supplementary material for "Approximating input-output curve of pumped storage hydro plant: A disjunctive convex hull method". [Online]. Available: https://github.com/ee-swang/supplementary-material/blob/main/SUPPL-TPWRS-00685-2021.pdf

Siyuan Wang received the B.S. and Ph.D. degrees in electrical engineering from the College of Electrical Engineering, Zhejiang University, Hangzhou, China, in 2013 and 2019, respectively. He is currently a Postdoctoral Fellow with the Department of Electrical and Computer Engineering, Missouri University of Science and Technology (formerly University of Missouri-Rolla), Rolla, MO, USA. His research interests include power system planning and operation, renewable energy integration, and applications of energy storage technology in power systems.

Jian Liu received the B.S. and M.S. degrees in Mathematics and System Engineering from Linyi University and Xiamen University, in 2005 and 2009, respectively. He is pursuing the Ph.D. degree at the Missouri University of Science and Technology, Rolla, Missouri. His current interests include power system operation, energy storage, and energy market.

Rui Bo (Senior Member, IEEE) received the BSEE and MSEE degrees in electric power engineering from Southeast University (China) in 2000 and 2003, respectively, and received the Ph.D. degree in electrical engineering from the University of Tennessee, Knoxville (UTK) in 2009. He is currently an Assistant Professor of the Electrical and Computer Engineering Department with the Missouri University of Science and Technology (formerly University of Missouri-Rolla). He worked as a Principal Engineer and Project Manager at Midcontinent Independent System Operator (MISO) from 2009 to 2017. His research interests include computation, optimization and economics in power system operation and planning, high performance computing, electricity market simulation, evaluation and design.

Yonghong Chen (Senior Member, IEEE) received the B.S. degree from Southeast University, Nanjing, China, the M.S. degree from Nanjing Automation Research Institute, China, and the Ph.D. degree from Washington State University, Pullman, WA, USA, all in electrical engineering. She also received the M.B.A. degree from Indiana University, Kelly School of Business, Indianapolis, IN, USA. She is currently a Consulting Advisor at MISO. In this role, she focuses on R&D to address challenges on market design and market clearing system. Before joining MISO in 2002, she worked with GridSouth Transco LLC and Nanjing Automation Research Institute.